International Journal of Engineering Science and Advanced Technology (IJESAT)
Vol 26 Issue 08, August 2026
Received: 25-06-2026 Accepted: 30-07-2026 Published: 05-08-2026

Seismic Performance Assessment of a G+25 RC Building Considering Soil–Structure Interaction, Outrigger Structural System, and Rubber Base Isolation Using NLTHA

Mohammed Yaqub[1], Ms. Khaja Begum[2], Dr A Swetha[3], Dr Mir Iqbal Faheem[4]

[1]Student, Department of Civil Engineering, Deccan college of Engineering and Technology, *Telangana, India*, mohdyaqub3030@gmail.com.

[2]*Assistant Professor, Department* of Civil Engineering, Deccan college of Engineering and Technology, *Telangana, India,:Khajabegum1865@gmail.com*

[3]*HOD, Department* of Civil Engineering, Deccan college of Engineering and Technology, *Telangana, India; swetha.swe112@gmail.com*

[4] *DIRECTOR, Department* of Civil Engineering, Deccan college of Engineering and Technology, *Telangana, India*

Abstract: This study evaluates the seismic performance of a symmetric G+25 storey reinforced concrete building located in Seismic Zone V (Z = 0.36, IS 1893:2016 Type II soil), across three structural configurations. Model A comprises a shear wall core with soil–structure interaction (SSI); Model B adds an outrigger structural system to Model A; and Model C further introduces rubber bearing base isolation. Seismic response is assessed using Equivalent Static Analysis (ESA), and Nonlinear Time History Analysis (NLTHA) under seven scaled ground motion records, implemented in ETABS. Model A exhibits the longest fundamental period (2.456 s) and the highest modal mass participation among the three configurations, but its inter-storey drift ratio under NLTHA exceeds the IS 1893:2016 limit at mid-height storeys. Model B reduces the fundamental period to 2.191 s and the equivalent static roof displacement by approximately 21%, moderating drift near the outrigger levels, though drift discontinuities persist between outrigger floors. Model C achieves the lowest roof displacement and the most uniform drift distribution over the building height, remaining within codal limits, and records the lowest P-Delta stability coefficient (θ = 0.0054) of the three models. Supplementary analyses show that wind loading (IS 875 Part 3:2015) contributes only about 9.3% of the seismic base shear and does not govern member design, while an indicative cost comparison shows Model B offering the most cost-efficient displacement control (+17.8% cost for a 21% displacement reduction) and Model C carrying a 41–77% cost premium justified primarily by its superstructure force-reduction benefit rather than by drift economy alone. Among the three configurations, Model C is the only one that satisfies the drift, stability, and modal mass participation provisions of IS 1893:2016 in their entirety.

Keywords: Soil–Structure Interaction; Outrigger Structural System; Rubber Bearing Base Isolation; Nonlinear Time History Analysis; Inter-Storey Drift Ratio; P-Delta Effect; ETABS2025.

I. Introduction

A. Background and Motivation

The accelerating pace of urbanization in Indian metropolitan centers has made vertical construction the dominant response to land scarcity, so that high-rise reinforced concrete (RC) buildings now form a substantial share of the residential and commercial building stock in cities such as Mumbai, Delhi, Hyderabad, Chennai, and Bengaluru. This growth has proceeded alongside a large seismic hazard, since a considerable fraction of the Indian landmass falls within Seismic Zones III, IV, and V as

2250-3676 ijesatj@gmail.com https://www.ijesat.com/

International Journal of Engineering Science and Advanced Technology (IJESAT)
Vol 26 Issue 08, August 2026
Received: 25-06-2026 Accepted: 30-07-2026 Published: 05-08-2026

defined by IS 1893:2016 (Part 1). Tall buildings are inherently sensitive to dynamic excitation because of their long natural periods, large tributary floor masses, and the substantial overturning moments that accumulate with height; when the natural period of the structure coincides with the dominant period of the ground motion, resonance can amplify the structural response several times beyond the static-equivalent estimate.

A further complication, often underappreciated in routine design, is the flexibility of the supporting soil. The conventional fixed-base idealization does not represent a structure founded on a deformable soil medium; soil–structure interaction (SSI) elongates the fundamental period, increases lateral displacement, and modifies the distribution of inter-storey drift and floor acceleration, particularly on soft-to-medium soils in high seismic zones. The choice of lateral force-resisting system compounds this complexity. Shear wall systems, while stiff and efficient up to moderate heights, accumulate large base overturning moments and boundary-element tension forces beyond approximately 20 storeys, motivating supplementary systems such as the outrigger structural, which mobilizes the axial stiffness of perimeter columns to relieve the core wall of overturning demand. Base isolation, using rubber bearings, offers a fundamentally different strategy, shifting the fundamental period of the building away from the dominant period range of typical earthquake ground motions rather than increasing the structure's capacity to resist seismic demand directly. Superimposed on all of these effects is the second-order P-Delta phenomenon, in which gravity loads acting through the laterally displaced position of the structure generate additional destabilizing moments; IS 1893:2016 both quantify this through a storey stability coefficient that must remain within prescribed limits.

While SSI, outrigger structural systems, base isolation, and P-Delta non linearity have each been investigated to varying degrees in isolation, a systematic evaluation of a realistic Indian high-rise RC building in which all four effects are considered simultaneously, within a single consistent analytical framework and benchmarked IS 1893:2016, is comparatively rare. This is significant given the increasing number of high-rise buildings being constructed on flexible soil deposits in Indian high seismic zones, and the growing, if still limited, adoption of outrigger and base-isolation systems. The present study addresses this gap through a G+25 storey RC building evaluated under three progressively more advanced structural configurations.

B. Seismic Setting and Structural Systems Considered

The building is analyzed for Seismic Zone V (Z = 0.36) with a design basic wind speed of 50 m/s, representing the most severe seismic demand scenario recognized under IS 1893:2016 (Part 1); Guwahati, Assam, is adopted as the notional site. Three lateral-system configurations are compared. Model A is a shear wall core system with SSI represented through spring–dashpot foundation elements. Model B augments Model A with an outrigger structural system, using box-section outriggers (500 × 500 × 30 mm) connecting the core to ISWB 350 trusses at the building perimeter. Model C further introduces a rubber bearing (RB) base isolation system, modeled as nonlinear link elements at the foundation, in addition to the outrigger system of Model B. This progress ion allows the incremental contribution of the outrigger system and of base isolation to be isolated and quantified against the SSI-only baseline.

C. Objectives

The specific objectives of the study are to: (i) quantify the influence of SSI, outrigger action, and base isolation on the fundamental period and modal mass participation of a G+25 RC building. (ii) compare storey displacement and inter-storey drift ratio under ESA, RSA, and NLTHA for the

2250-3676 ijesatj@gmail.com https://www.ijesat.com/

International Journal of Engineering Science and Advanced Technology (IJESAT)
Vol 26 Issue 08, August 2026
Received: 25-06-2026 Accepted: 30-07-2026 Published: 05-08-2026

three configurations against the IS 1893:2016 drift limit of 0.004.

(iii) evaluate the P-Delta stability coefficient and its sensitivity to the lateral system adopted.

(iv) characterize the near-fault pulse content of the ground motion suite used in the nonlinear analysis through signal-processing techniques.

(v) compare the seismic base shear against the wind base shear computed per IS 875 (Part 3):2015 to establish which load case governs member design

(vi) relate the incremental structural cost of the outrigger and isolation systems to their seismic performance benefit through an indicative cost–benefit comparison.

II. Literature Review

The published research most directly relevant to the four themes of the present study: soil–structure interaction (SSI) in high-rise reinforced concrete buildings, outrigger structural systems, rubber bearing base isolation, and second-order P-Delta geometric non-linearity under seismic loading. Rather than surveying the full body of literature, the review is limited to six studies (2018–2025) that most closely inform the modelling approach, analysis methodology, and research gap addressed by this thesis.

Markou et al. (2025) developed a high-performance computational framework for the three-dimensional nonlinear analysis of RC buildings, simultaneously incorporating SSI, base isolation, and geometric non-linearity. Applied to a 25-storey RC building, the study showed that neglecting any one of these three effects produced errors of up to 30% in peak storey drift, establishing that integrated modelling of the kind adopted in the present thesis is essential for reliable seismic performance prediction.

Chowdhury et al. (2024) compared outrigger systems with and without base isolation using nonlinear time history analysis under far-field and near-fault ground motions. The combination of outrigger and isolation produced the largest reduction in storey drift and base shear, with the outrigger controlling higher-mode response that the isolation system alone does not filter — a synergistic benefit exceeding the sum of the individual contributions.

Oz et al. (2023) compared the response of a 20-storey RC building under fixed-base and SSI conditions using nonlinear time history analysis with seven ground motion records. SSI was found to reduce base shear demand while amplifying roof displacement by up to 25% on soft soil, illustrating the dual and sometimes contradictory influence of SSI on different response parameters.

Kontoni et al. (2022) examined the SSI effect on base-isolated RC buildings with shear walls, comparing fixed-base, SSI, and SSI-isolated models. The SSI-isolated configuration gave the best seismic performance — reduced storey drift and floor acceleration — even on relatively soft soil, with shear walls found to be critical in limiting drift at upper storeys, directly supporting the dual-system approach adopted in this thesis.

Anand et al. (2021) conducted a parametric study on soil flexibility effects for RC frame buildings in Indian seismic zones III and IV, comparing fixed-base, Winkler spring, and direct-method SSI models. The Winkler spring-dashpot model was shown to reasonably approximate the direct method at a fraction of the computational cost, supporting its adoption for the SSI modelling used in the present study.

Lame et al. (2018) studied the optimum location of outrigger systems in tall buildings under seismic and wind loads using linear static and response spectrum analysis, concluding that an outrigger positioned at approximately 0.5H from the base maximizes the reduction in core bending moment and tip deflection a classical result that underpins the outrigger placement adopted in Models B and C of this thesis.

III. Methodology

A. Structural Models and Building Description

A G+25 storey RC building with a square plan of 20 m × 20 m and 4.0 m × 4.0 m bay spacing is modelled in ETABS. Floor-to-floor height is 3.2 m, giving a total height of 80 m. Member sizes are graded over three height zones to reflect the reduction in axial and flexural demand with height, as summarized in Table I. Three configurations sharing identical plan geometry,

2250-3676 ijesatj@gmail.com https://www.ijesat.com/

International Journal of Engineering Science and Advanced Technology (IJESAT)
Vol 26 Issue 08, August 2026
Received: 25-06-2026 Accepted: 30-07-2026 Published: 05-08-2026

floor height, and material properties are analyzed: Model A (SSI + shear wall core); Model B (SSI + shear wall + outrigger); and Model C (SSI + shear wall + outrigger + rubber bearing base isolation).

TABLE I. MEMBER SIZE SCHEDULE (WIDTH × DEPTH, mm)

Floor Zone	Inner Column	Peripheral Column	Beam Size
G to G+8	900 × 900	750 × 750	380 × 700
G+9 to G+18	750 × 750	600 × 600	380 × 600
G+19 to G+25	600 × 600	530 × 530	300 × 450

The outrigger structural system in Models B and C uses box-section outrigger members of 500 × 500 × 30 mm at strategically selected floor levels, tied together by ISWB 350 trusses encircling the building perimeter. The base isolation system in Model C uses rubber bearing elements modelled as nonlinear link supports, with a horizontal (U2) effective stiffness of 800 kN/m, nonlinear stiffness of 250 kN/m, yield strength of 80 kN, and a post-yield stiffness ratio of 0.1; the vertical (U3) direction retains a high effective stiffness of 1.5×10^7 kN/m to preserve gravity load transfer while permitting horizontal isolation.

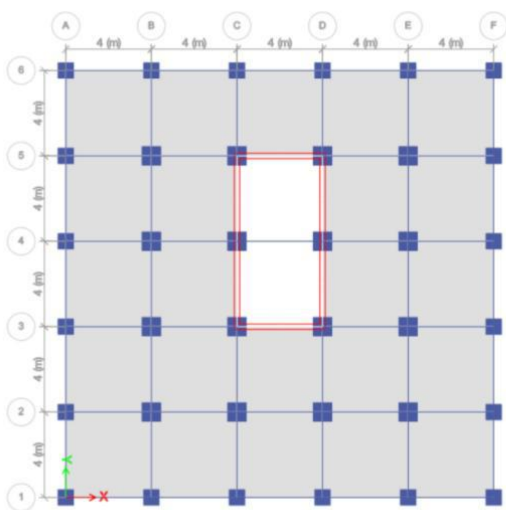

Fig. 1. Typical floor plan of the G+25 building, showing the column grid and central shear wall core.

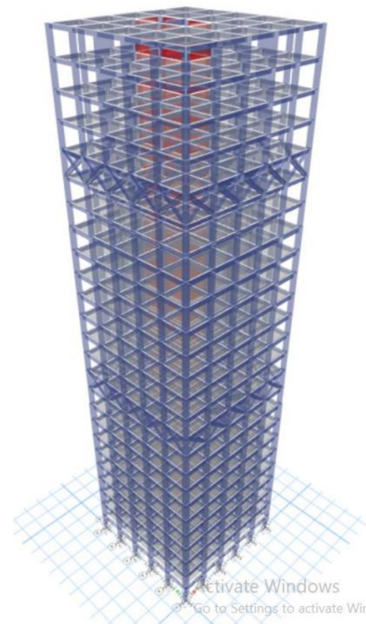

Fig. 2. Three-dimensional ETABS model of the structural system, including the outrigger levels.

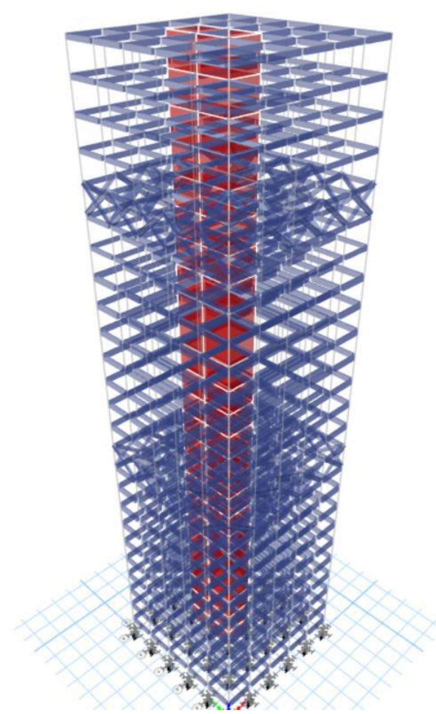

Fig. 3. Three-dimensional model incorporating soil–structure interaction (SSI) through spring-link foundation elements.

2250-3676 ijesatj@gmail.com https://www.ijesat.com/

International Journal of Engineering Science and Advanced Technology (IJESAT)
Vol 26 Issue 08, August 2026
Received: 25-06-2026 Accepted: 30-07-2026 Published: 05-08-2026

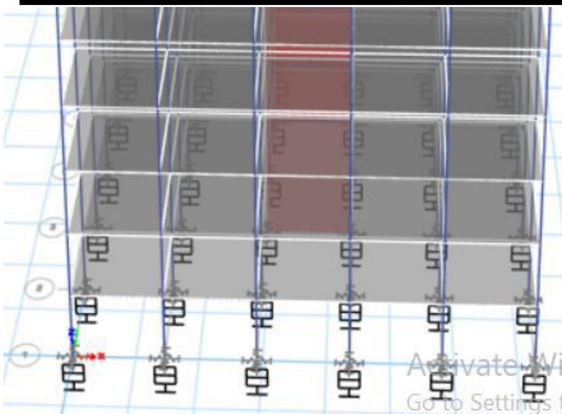

Fig. 4. Rubber bearing base-isolation link elements at the foundation level, Model C.

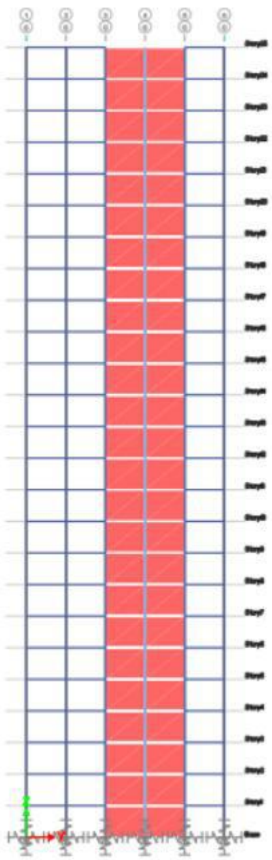

Fig. 5. Elevation view of the 3D model showing the SSI foundation and outrigger levels.

B. Gravity Load

Loads are computed per IS 875 (Parts 1, 2, and 3):1987 using the tributary area method for a 150 mm slab, with a superimposed dead load of 1.0–3.0 kN/m² and a residential live load of 3.0 kN/m², combined with a masonry wall load transferred to supporting beams. Table II summarizes the principal gravity load assumptions common to all three models.

TABLE II. GRAVITY LOAD

Parameter	Value
Slab thickness	150 mm
Unit weight of concrete	25 kN/m³
Floor finish / superimposed DL	1.0–3.0 kN/m² (IS 875 Pt.1)
Live load (residential)	3.0 kN/m² (IS 875 Pt.2)
Masonry wall thickness	230 mm
Design basic wind speed	50 m/s (IS 875 Pt.3:2015)

C. Seismic Analysis Methods

Three levels of seismic analysis are carried out for each model: Equivalent Static Analysis (ESA) and Response Spectrum Analysis (RSA) per IS 1893 (Part 1):2016, and Nonlinear Time History Analysis (NLTHA) under seven ground motion records drawn from the PEER NGA-West2 database and scaled to the Zone V design spectrum (Z = 0.36). Rigid diaphragm action is assigned at every floor level, and mass source combines 100% dead load with the appropriate fraction of live load per IS 1893:2016. Load combinations follow the code-prescribed factored combinations of dead, live, seismic, and (where applicable) wind load cases; IS 1893 (Part 1):2016 Clause 6.3.1.2 requires that wind and seismic loads be considered in separate, non-concurrent combinations.

D. P-Delta Stability Formulation

Second-order geometric non linearity is evaluated through the storey stability coefficient

$$\theta = (\Sigma P_i \times \Delta_i) / (V_i \times h_i)$$

where ΣP_i is the total factored gravity load above storey i, Δ_i is the inter-storey drift, V_i is the storey shear, and h_i is the storey height, using the iterative P-Delta method under a gravity combination of 100% dead load plus 25% live load. $\theta \leq 0.10$ indicates that P-Delta effects may be neglected, $0.10 < \theta \leq 0.25$ requires an amplification factor of $1/(1-\theta)$ on drift and moment, and $\theta > 0.25$ indicates a potentially unstable structure requiring redesign.

2250-3676 ijesatj@gmail.com https://www.ijesat.com/

International Journal of Engineering Science and Advanced Technology (IJESAT)
Vol 26 Issue 08, August 2026
Received: 25-06-2026 Accepted: 30-07-2026 Published: 05-08-2026

E. Ground Motion Signal Processing

Five strong-motion horizontal and vertical components, drawn from the 1999 Chi-Chi (station TCU102) and 1999 Düzce earthquakes, are processed to characterize near-fault pulse content. Each record is baseline-corrected and integrated to obtain velocity and displacement time histories, from which peak ground acceleration (PGA), peak ground velocity (PGV), peak ground displacement (PGD), and the PGV/PGA ratio are computed. A continuous wavelet transform (Morlet) is applied to the velocity time history to extract a dominant velocity pulse, yielding a pulse ratio and dominant pulse period used to screen each record for pulse-like character; 5%-damped elastic pseudo-acceleration and pseudo-velocity response spectra are computed for each record.

F. Wind Load Methodology

Storey-wise design wind pressure and force are computed by the static method of IS 875 (Part 3):2015 for a basic wind speed of 50 m/s and Terrain Category 2, using the height-and-terrain multiplier k_2 to obtain the design wind speed V_r and pressure p_r at each storey, from which the storey wind force F_γ is derived from the tributary exposed area. The resulting total wind base shear is compared against the NLTHA seismic base shear common to all three models (equal seismic weight and zone classification).

G. Cost–Benefit Methodology

An indicative, order-of-magnitude structural cost comparison is developed from a quantity take-off of concrete (M25), reinforcement (Fe500D TMT), and structural steel (outrigger box sections and ISWB 350 trusses), priced at representative unit rates. The incremental cost of Model B over Model A reflects the additional outrigger/truss steel; the incremental cost of Model C over Model B reflects an assumed isolation-system premium, which is treated parametrically over a 20–50% range given the absence of a verified, project-specific benchmark for this building class and isolator configuration.

IV. Results and Discussion

A. Modal Properties

SSI elongates the fundamental period of Model A to 2.456 s, with cumulative modal mass participation reaching 94.15% by Mode 11. The outrigger system in Model B increases lateral stiffness sufficiently to reduce the fundamental period to 2.191 s while satisfying the 90% mass-participation requirement by Mode 12. Model C records a fundamental period of 2.197 s and 91.62% modal mass participation by Mode 10, reflecting the combined effect of isolation-induced period lengthening at the isolation interface and outrigger-induced stiffening of the superstructure above it.

B. Storey Displacement and Inter-Storey Drift

Table III summarizes the comparative modal, displacement, drift, shear, and stability results for the three models, consolidated from the ESA, RSA, and NLTHA analyses.

TABLE III. SEISMIC PERFORMANCE SUMMARY — MODELS A, B, AND C

Parameter	Model A (SSI)	Model B (SSI+Outrigger)	Model C (SSI+Outrigger+RB)
Fundamental period (s)	2.456	2.191	2.197
Modal mass participation	94.15 % (Mode 11)	>90% (Mode 12)	91.62% (Mode 10)
Max. roof displacement, ESA (mm)	135.58	– (reduced)	107.70 (lowest)
Max. roof displacement, EQ-X (mm)	90.38	71.46 (−21%)	lowest of the three
Max. roof displacement, RSA (mm)	48.81	reduced	further reduced

2250-3676 ijesatj@gmail.com https://www.ijesat.com/

International Journal of Engineering Science and Advanced Technology (IJESAT)
Vol 26 Issue 08, August 2026
Received: 25-06-2026 Accepted: 30-07-2026 Published: 05-08-2026

Parameter	Model A (SSI)	Model B (SSI+Outrigger)	Model C (SSI+Outrigger+RB)
Avg. NLTHA roof displacement +X/−X (mm)	339.17 / −301.46	significantly reduced	lowest (isolation absorbs demand)
Max. drift ratio, X-direction	0.00656 (Storey 20)	reduced near outriggers	0.005786 (Storey 19)
Max. drift ratio, Y-direction	0.00556 (Storey 24)	reduced at mid-height	0.004921 (Storey 17)
IS 1893:2016 drift compliance	Non-compliant	Partially compliant	Compliant / near-compliant
Max. base shear +X/−X, Storey shear(kN)	40,757 / −32,253	similar to Model A	similar at isolation level; reduced above
P-Delta stability coefficient θ	< 0.10	< 0.10	0.0054
Overall seismic performance rank	3	2	1

IS 1893:2016 permissible inter-storey drift ratio = 0.004; P-Delta stability threshold $\theta \leq 0.10$. Values derived from ESA, RSA, and NLTHA (seven scaled ground motion records; the governing record for displacement and shear is common across all three models). Base shear is broadly comparable across models owing to equal seismic weight and zone classification; the *distinguishing factor lies in the distribution of shear within the superstructure.*

Model A displays cantilever-type deformation with drift concentrated at storeys 18–22, exceeding the code limit at mid-height. The outrigger system in Model B reduces displacement and introduces a kink in the deformed shape at the outrigger levels, but this stiffness discontinuity concentrates drift at the storeys immediately adjacent to the outriggers, so that peak drift remains marginally above the codal limit even though overall displacement is reduced by roughly one-fifth. Model C exhibits an almost rigid-body response above the isolation interface, with deformation concentrated at the isolation plane itself; this produces both the lowest roof displacement and the most uniform drift distribution over the building height, the only configuration that remains within the 0.004 limit throughout.

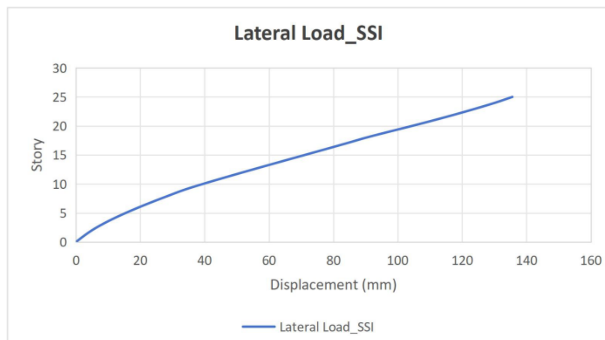

Fig. 6. Storey displacement profile under lateral (equivalent static) load, Model A (SSI with shear wall).

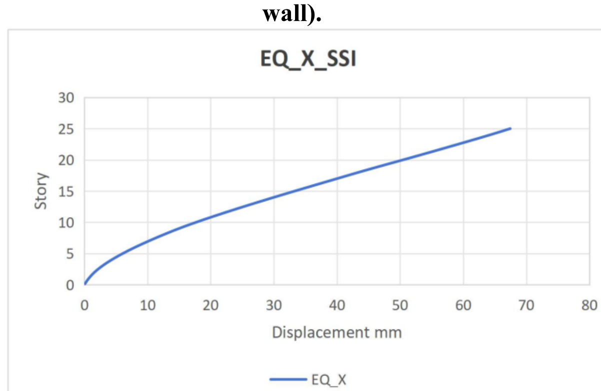

Fig. 7. Storey displacement profile under earthquake load EQ-X, Model A.

2250-3676 ijesatj@gmail.com https://www.ijesat.com/

International Journal of Engineering Science and Advanced Technology (IJESAT)
Vol 26 Issue 08, August 2026
Received: 25-06-2026 Accepted: 30-07-2026 Published: 05-08-2026

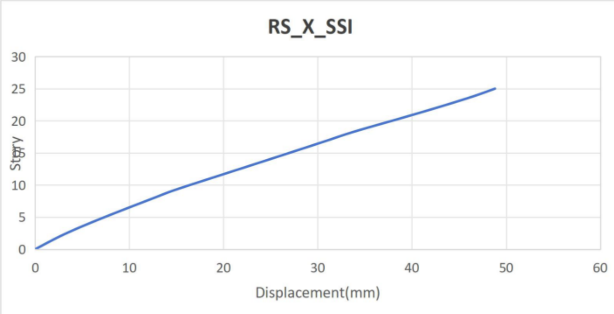

Fig. 8. Storey displacement profile under response spectrum analysis (RSX), Model A.

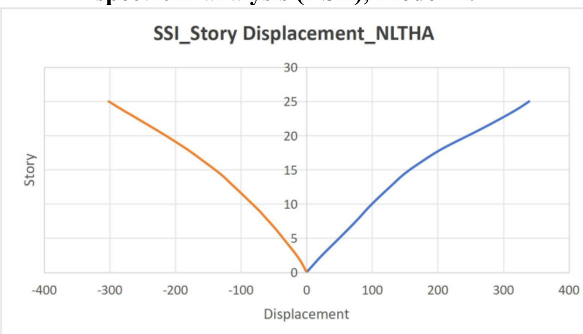

Fig. 9. Average storey displacement profile under NLTHA, Model A.

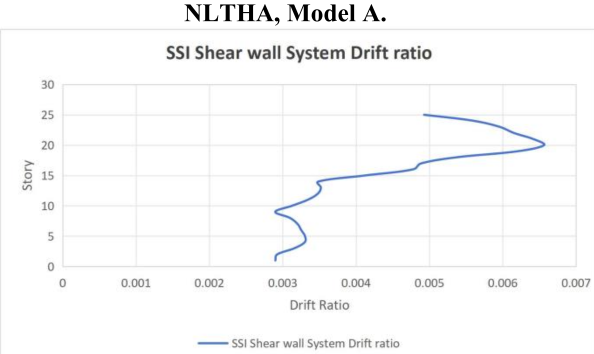

Fig. 10. Storey drift ratio in the X-direction, Model A.

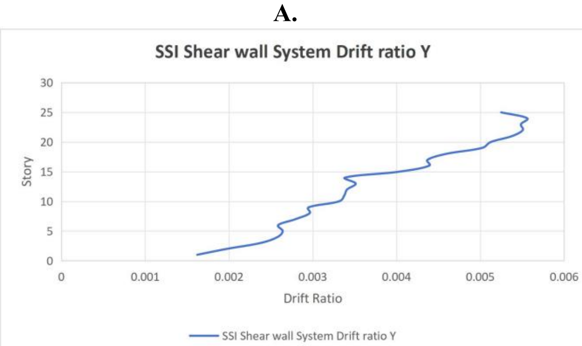

Fig. 11. Storey drift ratio in the Y-direction, Model A.

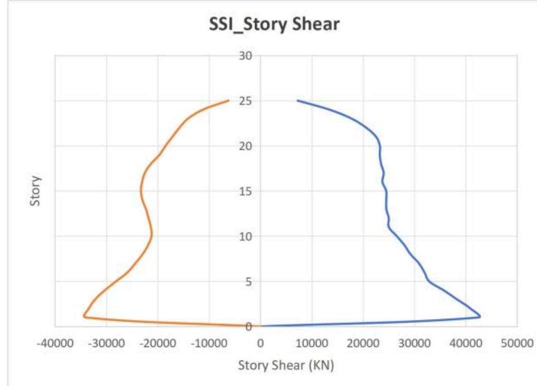

Fig. 12. Average storey shear force profile under NLTHA, Model A.

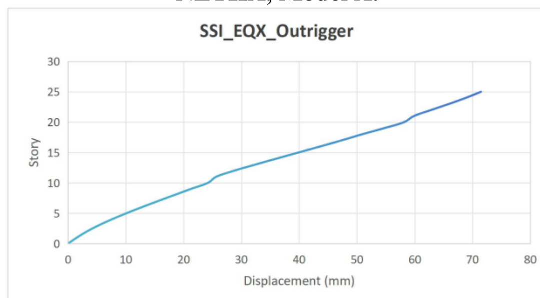

Fig. 13. Storey displacement profile under EQ-X, Model B (SSI with shear wall and outrigger).

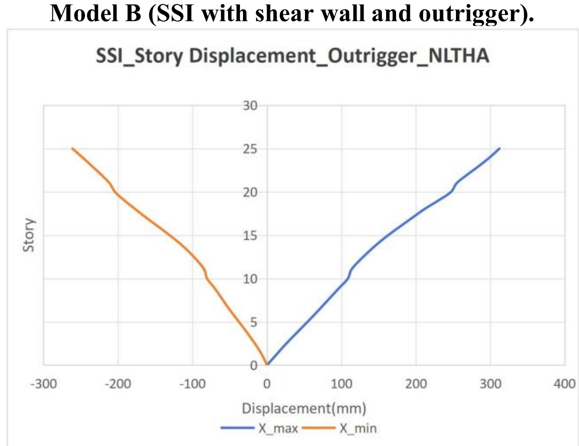

Fig. 14. Average storey displacement profile under NLTHA, Model B.

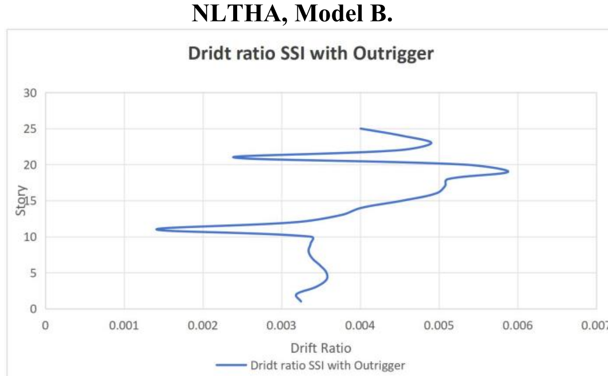

2250-3676 ijesatj@gmail.com https://www.ijesat.com/

International Journal of Engineering Science and Advanced Technology (IJESAT)
Vol 26 Issue 08, August 2026
Received: 25-06-2026 Accepted: 30-07-2026 Published: 05-08-2026

Fig. 15. Storey drift ratio in the X-direction, Model B, showing the characteristic dip at outrigger levels.

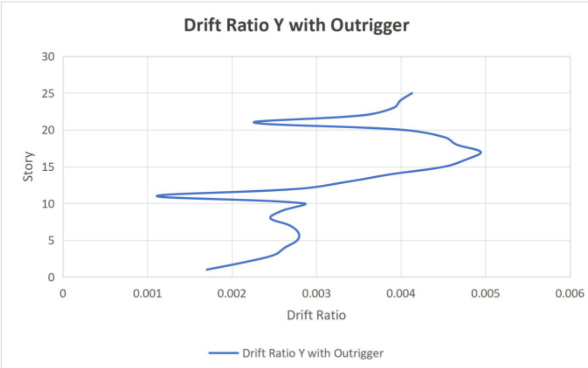

Fig. 16. Storey drift ratio in the Y-direction, Model B.

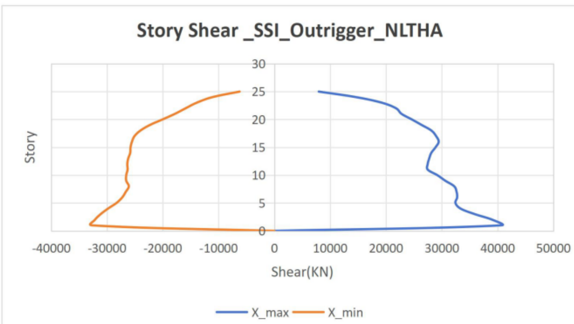

Fig. 17. Average storey shear force profile under NLTHA, Model B.

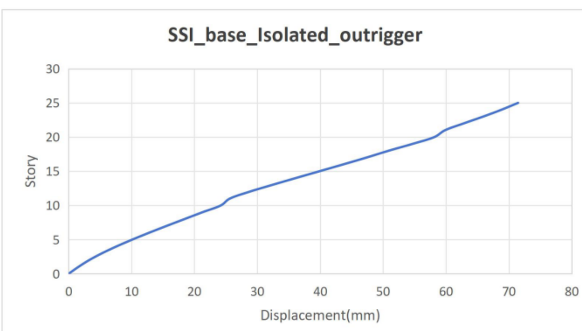

Fig. 18. Storey displacement profile under linear analysis, Model C (base-isolated SSI).

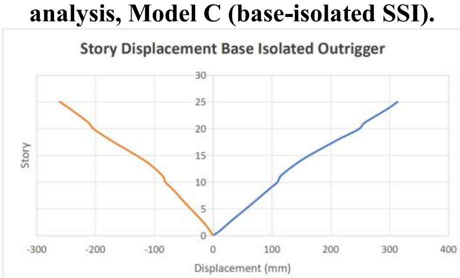

Fig. 19. Average storey displacement profile under NLTHA, Model C.

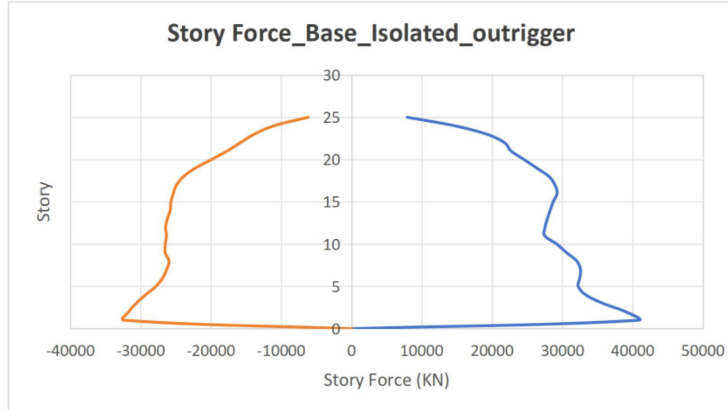

Fig. 20. Average storey force profile under NLTHA, Model C.

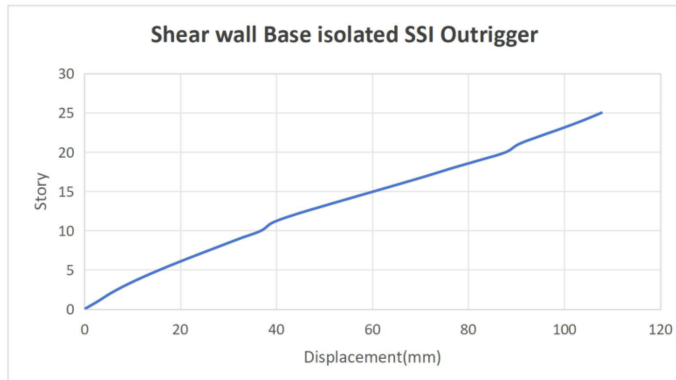

Fig. 21. Storey shear profile, Model C, contrasted with the fixed-base/SSI-only response.

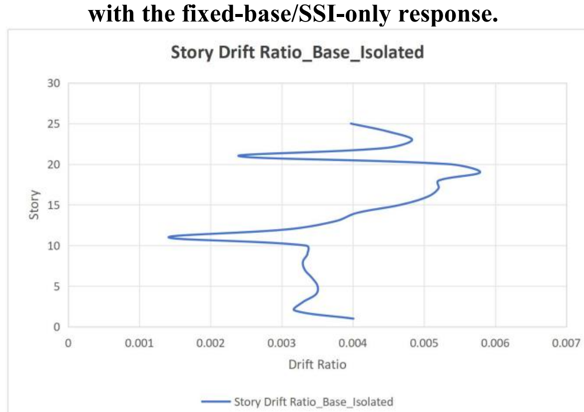

Fig. 22. Storey drift ratio in the X-direction, Model C, showing uniformly reduced drift.

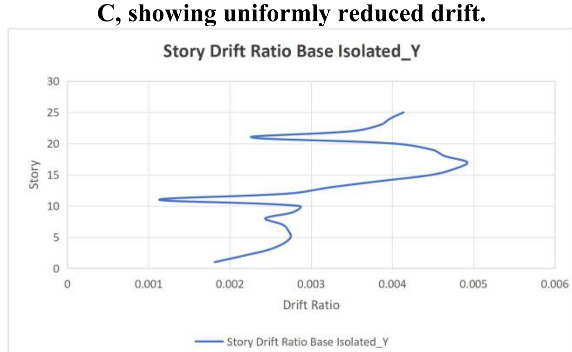

2250-3676 ijesatj@gmail.com https://www.ijesat.com/

International Journal of Engineering Science and Advanced Technology (IJESAT)
Vol 26 Issue 08, August 2026
Received: 25-06-2026 Accepted: 30-07-2026 Published: 05-08-2026

Fig. 23. Storey drift ratio in the Y-direction, Model C.

C. P-Delta Stability

All three models satisfy the IS 1893:2016/ASCE 7 stability criterion ($\theta \leq 0.10$), confirming that second-order effects do not threaten global stability in any configuration. Model C nonetheless records the lowest stability coefficient (0.0054), an order of magnitude below the threshold, reflecting the compounding benefit of reduced drift from both the outrigger and the isolation system acting together.

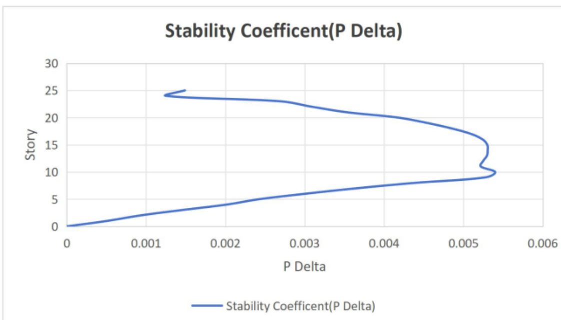

Fig. 24. Storey-wise P-Delta stability coefficient (θ), compared across the building height.

D. Near-Fault Pulse Characterisation

Table IV summarizes the computed ground-motion intensity parameters for the five processed strong-motion components. PGA values range from approximately 0.17 g to 0.51 g, PGV from 66 to 92 cm/s, and PGD from 44 to 104 cm. The two horizontal components at TCU102 (Chi-Chi) show the highest PGV/PGA ratios (≈ 0.31–0.39 s) of the set, consistent with long-period, forward-directivity character, while the Düzce components show comparatively lower ratios (≈ 0.17–0.18 s) despite higher PGA, indicating higher-frequency content. Although none of the five records exceeded the simplified wavelet pulse-ratio screening threshold applied in this study, the TCU102-V and DZC180 components produced the highest pulse ratios and the longest extracted pulse periods (3.6–3.8 s), broadly consistent with the pulse-like character reported for these events elsewhere in the literature — a discrepancy that illustrates the conservatism of the simplified screening procedure relative to more elaborate published methods, rather than a genuine absence of pulse character in these records.

TABLE IV. COMPUTED GROUND-MOTION PARAMETERS

Record	PGA (g)	PGV (cm/s)	PGD (cm)	PGV/PGA (s)	Pulse Ratio	Pulse Period (s)
TCU102-E (Chi-Chi, 1999)	0.304	91.72	104.25	0.308	0.043	1.93
TCU102-N (Chi-Chi, 1999)	0.172	66.43	50.70	0.394	0.311	1.97
TCU102-V (Chi-Chi, 1999)	0.177	68.43	51.83	0.394	0.548	3.64
DZC180 (Düzce, 1999)	0.404	71.33	44.32	0.180	0.163	3.78
DZC270 (Düzce, 1999)	0.515	84.20	47.51	0.167	0.074	1.75

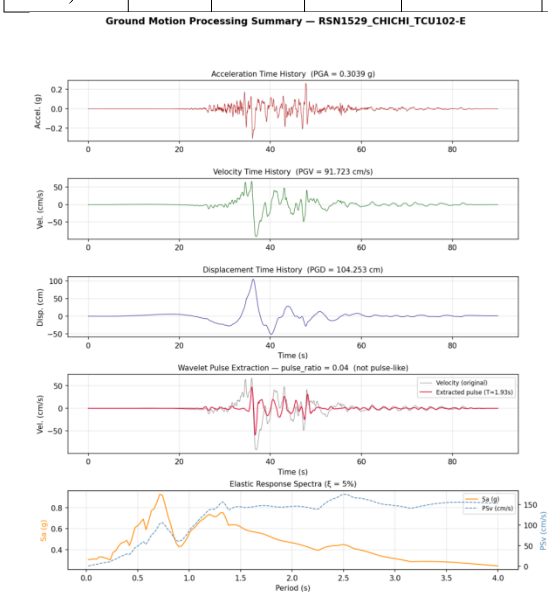

Fig. 25. Ground-motion processing summary for record TCU102-E (Chi-Chi, 1999), East-West component.

2250-3676 ijesatj@gmail.com https://www.ijesat.com/

Received: 25-06-2026 Accepted: 30-07-2026 Published: 05-08-2026

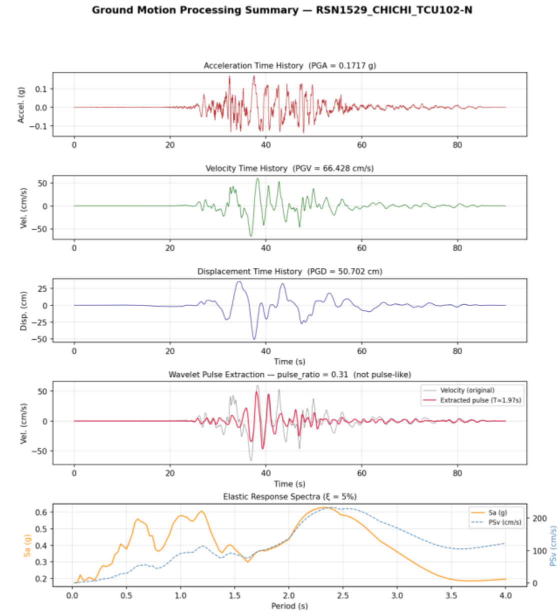

Fig. 26. Ground-motion processing summary for record TCU102-N (Chi-Chi, 1999), North-South component.

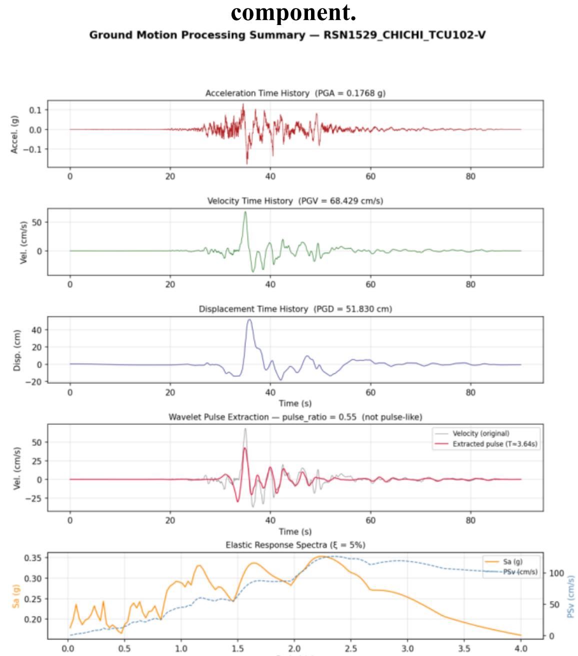

Fig. 27. Ground-motion processing summary for record TCU102-V (Chi-Chi, 1999), Vertical component.

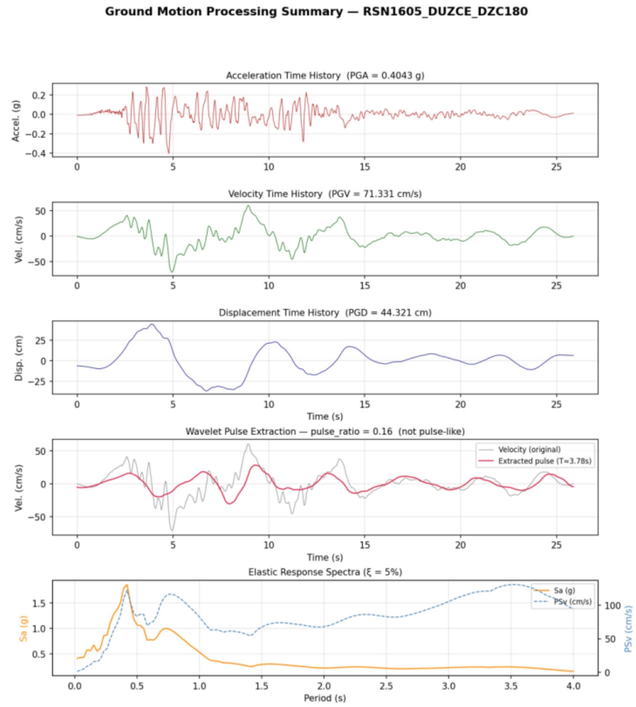

Fig. 28. Ground-motion processing summary for record DZC180 (Düzce, 1999), 180° horizontal component.

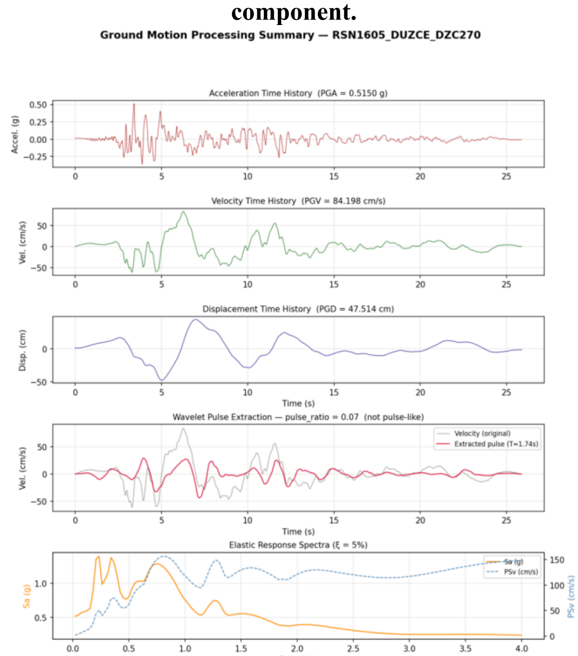

Fig. 29. Ground-motion processing summary for record DZC270 (Düzce, 1999), 270° horizontal component.

E. Wind versus Seismic Demand

Table V compares the total wind base shear, computed by the static method of IS 875 (Part 3):2015, against the governing seismic base shear from NLTHA. The wind pressure profile

2250-3676 ijesatj@gmail.com https://www.ijesat.com/

International Journal of Engineering Science and Advanced Technology (IJESAT)
Vol 26 Issue 08, August 2026
Received: 25-06-2026 Accepted: 30-07-2026 Published: 05-08-2026

increases from about 1,500 N/m² near the base to roughly 2,193 N/m² at roof level, an increase of about 46% over the building height consistent with Terrain Category 2. The storey force distribution mirrors the pressure profile rather than the sharply tapered pattern seen under seismic loading, which is governed instead by the fundamental mode shape and storey mass.

TABLE V. WIND VERSUS SEISMIC BASE SHEAR

Load Case	Base Shear (kN)	Basis
Wind (WX = WY, static method)	3,803	IS 875 (Part 3):2015
Seismic NLTHA (avg. max., governing record)	40,757	Common to Models A, B, C
Wind as % of seismic base shear	9.3%	–

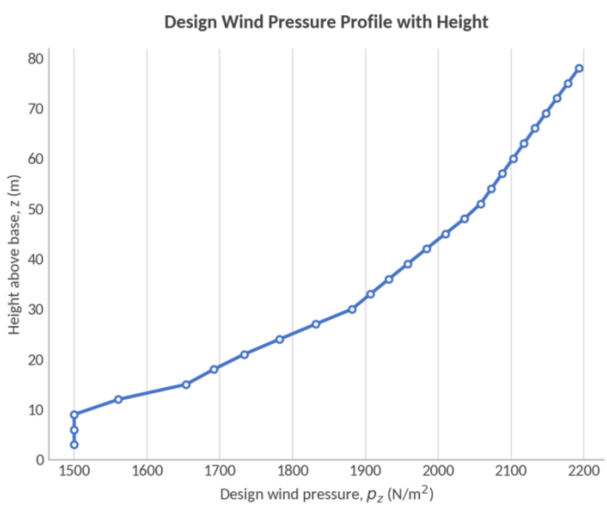

Fig. 30. Design wind pressure profile with building height (IS 875 Part 3:2015, static method).

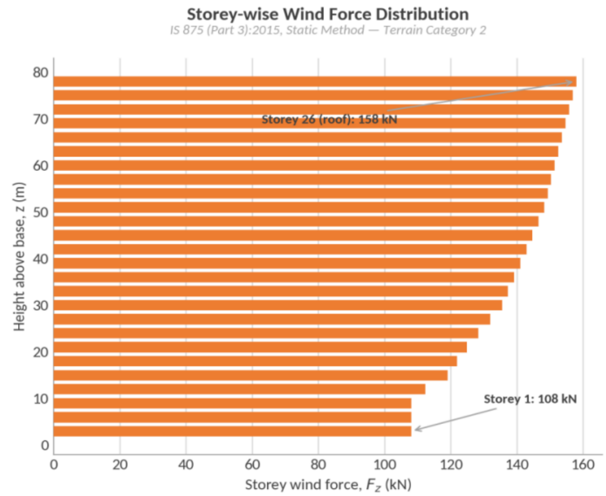

Fig. 31. Storey-wise wind force distribution.

.

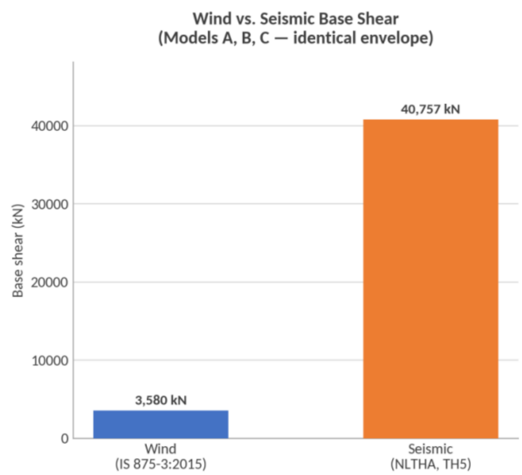

Fig. 32. Comparison of total wind base shear against the governing seismic (NLTHA) base shear.

Seismic action governs the lateral design of the building by a wide margin, consistent with expected behaviour for a Zone V structure with a moderate basic wind speed; the outrigger, belt-truss, and isolator elements sized against seismic demand therefore carry comfortable reserve capacity against the wind load case, and need not be re-checked against the wind combination.

F. Cost Benefit Comparison

Table VI presents the indicative structural cost comparison of the three configurations, based on the quantity take-off of concrete, reinforcement, and structural steel described in Section III.G.

2250-3676 ijesatj@gmail.com https://www.ijesat.com/

International Journal of Engineering Science and Advanced Technology (IJESAT)
Vol 26 Issue 08, August 2026
Received: 25-06-2026 Accepted: 30-07-2026 Published: 05-08-2026

TABLE VI. INDICATIVE STRUCTURAL COST COMPARISON

Model	Structural Cost	Premium over Model A	Basis
Model A — SSI + Shear Wall	Rs. 7.92 Cr	– (baseline)	Concrete + reinforcement only
Model B — SSI + Shear Wall + Outrigger	Rs. 9.34 Cr	+17.8%	Model A + outrigger\ truss steel
Model C — SSI + Shear Wall + Outrigger + RB Isolation	Rs. 12.60 Cr	+59.1%	Model B + 35% isolation premium (base case)

Model B offers a favourable cost-to-benefit ratio for displacement control: roughly 1.2% additional cost per 1% reduction in equivalent static roof displacement (+17.8% cost for a 21% displacement reduction). Model C carries the largest premium, and its 35% isolation-system cost assumption is not independently verified; treated parametrically over a 20–50% premium range, Model C's total premium over Model A varies from roughly +41% to +77%, which does not change the qualitative conclusion that Model C is the costliest configuration under any reasonable assumption. Model C's benefit is not, however, fully captured by drift reduction alone: base isolation fundamentally changes the load path, concentrating deformation at the isolation plane and substantially reducing force demand on beams, columns, and connections throughout the superstructure. This benefit more accurately measured by reduced member forces and reduced reinforcement congestion than by drift ratio alone would typically justify Model C where continued-operation performance is required (e.g., hospitals, data centers, or other critical facilities), rather than on drift-ratio economy alone.

G. Storey-wise Overturning Moment

Figures 24–31 present the variation of storey-wise overturning moment with building elevation for the governing gravity, seismic, load-combination, and modal load cases, extracted directly from the structural analysis output about both principal axes.

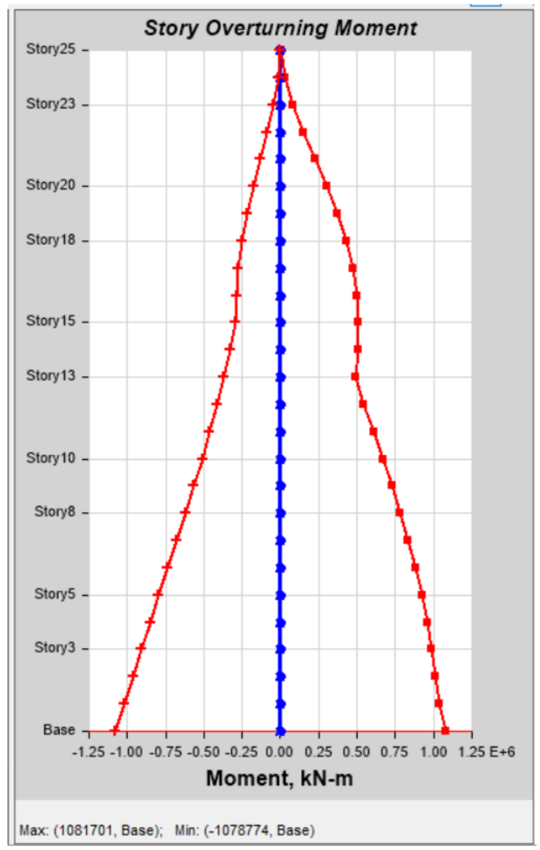

Fig. 39. Envelope of maximum and minimum overturning moment with storey elevation, load combination LC-1.

2250-3676 ijesatj@gmail.com https://www.ijesat.com/

International Journal of Engineering Science and Advanced Technology (IJESAT)
Vol 26 Issue 08, August 2026
Received: 25-06-2026 Accepted: 30-07-2026 Published: 05-08-2026

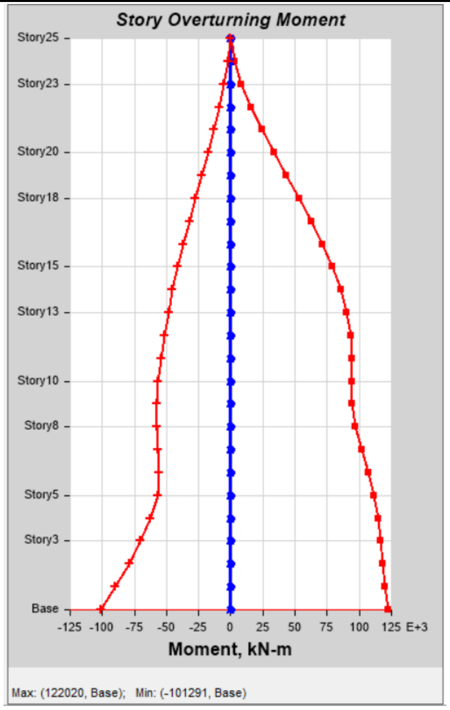

Fig. 40. Envelope of maximum and minimum overturning moment with storey elevation, load combination LC-2.

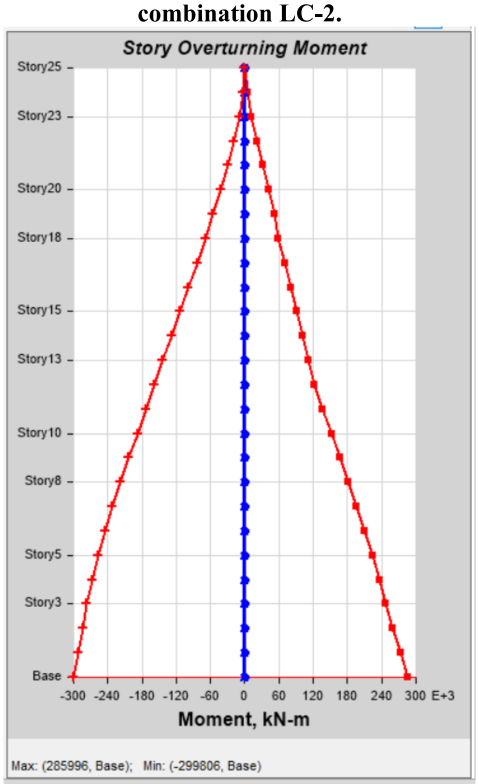

Fig. 41. Envelope of maximum and minimum overturning moment with storey elevation, load combination LC-3.

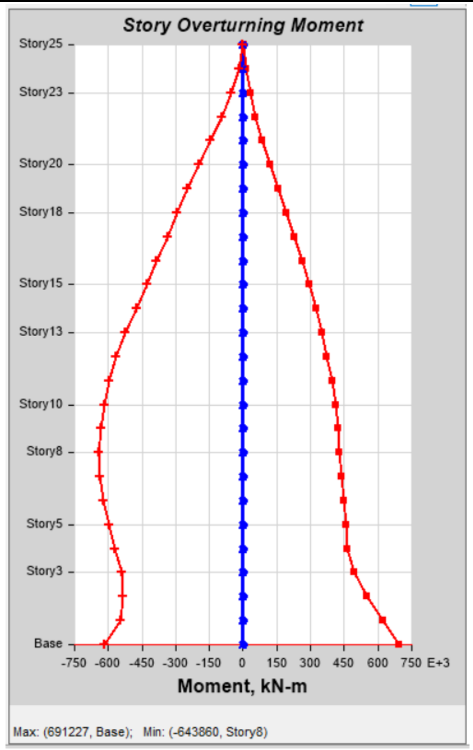

Fig. 42. Envelope of maximum and minimum overturning moment with storey elevation, load combination LC-4.

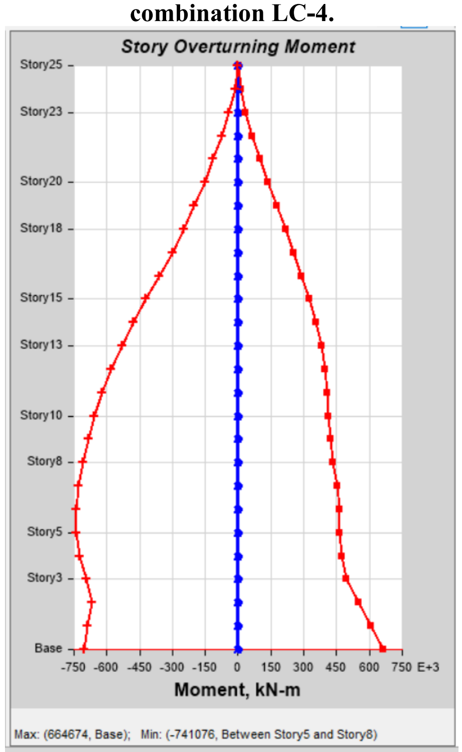

Fig. 43. Envelope of maximum and minimum overturning moment with storey elevation, load combination LC-5.

V. Conclusions

2250-3676 ijesatj@gmail.com https://www.ijesat.com/

Received: 25-06-2026 Accepted: 30-07-2026 Published: 05-08-2026

1) Model A (SSI with shear wall core): SSI elongates the fundamental period to 2.456 s, with 94.15% cumulative modal mass participation by Mode 11. Maximum roof displacements of 135.58 mm (ESA), 48.81 mm (RSA), and 339.17 mm (NLTHA) confirm the significant influence of SSI on the seismic response of the G+25 RC building, and its peak inter-storey drift exceeds the IS 1893:2016 limit at mid-height storeys.

2) Model B (SSI + outrigger): the outrigger system reduces equivalent static roof displacement by approximately 21% and increases lateral stiffness, reducing the fundamental period to 2.191 s. Peak drift remains marginally above the IS 1893:2016 limit owing to stiffness discontinuity at outrigger levels, while the P-Delta coefficient ($\theta < 0.10$) confirms adequate second-order stability.

3) Model C (SSI + outrigger + rubber bearing isolation): the integrated system achieves a 2.197 s fundamental period and 91.62% modal mass participation by Mode 10. NLTHA results show the lowest roof displacement and storey drift of the three configurations, through isolation-level deformation concentration and the lowest recorded stability coefficient ($\theta = 0.0054$).

4) Overall, Model C provides the most effective seismic performance among the three configurations, reducing NLTHA roof displacement by 20–35% relative to Model A while remaining within IS 1893:2016 drift limits throughout the building height. Wind effects are non-governing (9.3% of the seismic base shear) for all three models. Despite a 41–77% structural cost premium over the baseline, the integrated outrigger–isolation system (Model C) is, of the three configurations examined, the only one that satisfies the drift, stability, and modal mass-participation provisions of IS 1893:2016 in their entirety, and represents the most effective seismic solution for G+25 RC buildings on flexible soil in high seismic zones among the options considered.

Future Scope

Future work may extend this framework to buildings with plan or vertical irregularities and varying height and aspect ratio; incorporate nonlinear soil behaviour, cyclic degradation, liquefaction potential, and foundation gapping into the SSI model; compare rubber bearings against lead-rubber, high-damping rubber, and friction pendulum isolators; systematically optimize outrigger location and stiffness distribution; and employ a larger ground-motion suite to improve the statistical robustness of the nonlinear time history results.

References

1. Markou, A. A., & Gendy, B. L. (2025). A high-performance computational framework for nonlinear soil–structure–isolation interaction analysis of RC buildings. Engineering Structures.
2. Chowdhury, S., et al. (2024). Comparative performance of outrigger systems with and without base isolation under near-fault and far-field ground motions. Journal of Building Engineering.
3. Oz, I., et al. (2023). Fixed-base versus soil–structure interaction response of a 20-storey RC building under nonlinear time history analysis. Applied Sciences.
4. Kontoni, D.-P. N., & Farghaly, A. A. (2022). Soil–structure interaction effects on the seismic response of base-isolated RC shear wall buildings. Coupled Systems Mechanics.
5. Anand, V., & Kumar, R. (2021). Parametric evaluation of soil flexibility models for RC frame buildings in Indian seismic zones III and IV. Structures.
6. Lame, A., & Balasaheb, K. (2018). Optimum location of outrigger systems in tall buildings under seismic and wind loads. International Journal of Civil Engineering and Technology.

2250-3676 ijesatj@gmail.com https://www.ijesat.com/